

INTERNATIONAL ATOMIC ENERGY AGENCY
UNITED NATIONS EDUCATIONAL, SCIENTIFIC AND CULTURAL ORGANIZATION



INTERNATIONAL CENTRE FOR THEORETICAL PHYSICS
34100 TRIESTE (ITALY) · P.O.B. 586 · MIRAMARE · STRADA COSTIERA 11 · TELEPHONES: 224281/2/3/4/5-6
CABLE: CENTRATOM - TELEX 460392-1

SMR/108-7

WORKSHOP ON NUCLEAR MODEL COMPUTER CODES

16 January - 3 February 1984

CALCULATING FISSION CROSS SECTIONS USING NUCLEAR MODELS

F. MANN

Hanford Engineering Development Laboratory
Richland, Washington
U.S.A.

These are preliminary lecture notes, intended only for distribution to participants.
Missing or extra copies are available from Room 231.

COURSE OUTLINE

I. Introduction

- A. What do we want to calculate
- B. What we will and will not cover
- C. How we will cover material

II. Fission Theory

- A. Classical Picture
- B. Theoretical Basis of Double Hump Barrier
- C. Implications of Double Hump Barrier

III. Calculation of Fission Transmission Coefficient

- A. Single Hump Barrier
- B. WKB approximation
- C. Double Hump Barrier

IV. Experimental Determination of Parameters

- A. Level density parameters

B. Barrier widths

- C. Barrier heights

V. Actual Fission Calculations

- A. Direct reactions
- B. Neutron-induced
- C. Systematics

CALCULATING FISSION CROSS SECTIONS

USING NUCLEAR MODELS

FRED MANN

HANFORD ENGINEERING DEVELOPMENT LABORATORY

RICHLAND, WASHINGTON, U.S.A.

REVIEWS

1. S. Bjornholm and J.E. Lynn, "The Double-Humped Fission Barrier", Reviews of Modern Physics 52(1980)725-932.
2. A. Michaudon, "Nuclear Fission", Advances in Nuclear Physics 6(1973)1.

12. J. E. Behrens, Trans. Am. Nucl. Soc. 44(1983)243, systematics of fission cross sections.

HISTORICAL REFERENCES

1. O. Hahn and F. Strassman, Naturwissenschaften 27(1939)11, discovery of fission.
2. W. J. Swiatecki, Physics Review 100(1955)937, shell effects first proposed to explain properties of fission.
3. V.M. Strutinsky, Nuclear Physics A95, (1967)420, calculated shell effects.
4. N. Bohr and J. Wheeler, Phys. Rev. 56(1939)426, first calculation of barrier heights from macroscopic approach.
5. D. L. Hill and J. A. Wheeler, Phys. Rev. 89(1953)1102, description of fission through use of an inverted harmonic oscillator.
6. A. Bohr, Proc. Int. Conf. Peaceful Uses of Atomic Energy (Geneva, 1955) Vol. II, United Nations, New York, 1956, p. 220.
7. S. Polikanov, et al., Sov. Phys. - JETP 15(1962)1016, discovery of fission isomer.
8. J. E. Lynn, Nuclear Structure, I.A.E.A., Vienna, (1968) p. 463, and J. E. Lynn, A.E.R.E. Report R589, Harwell (1968), class I and II states as result of double hump barrier.
9. M. Brack, et al., Rev. Mod. Phys. 44(1972)320, justification, technical method and physical nature of Strutinsky's method.
10. D. G. Madland and J. R. Nix, Nucl. Sci. J. Eng. 81(1982)213, description of method of calculating prompt fission neutron spectrum and multiplicities.
11. E. D. Arthur, P. G. Young, D. G. Madland and R. E. MacFarlane, LA-9873-MS Los Alamos National Laboratory, description of methods used in ^{239}Pu ENDF/B-V evaluation (revision 2).

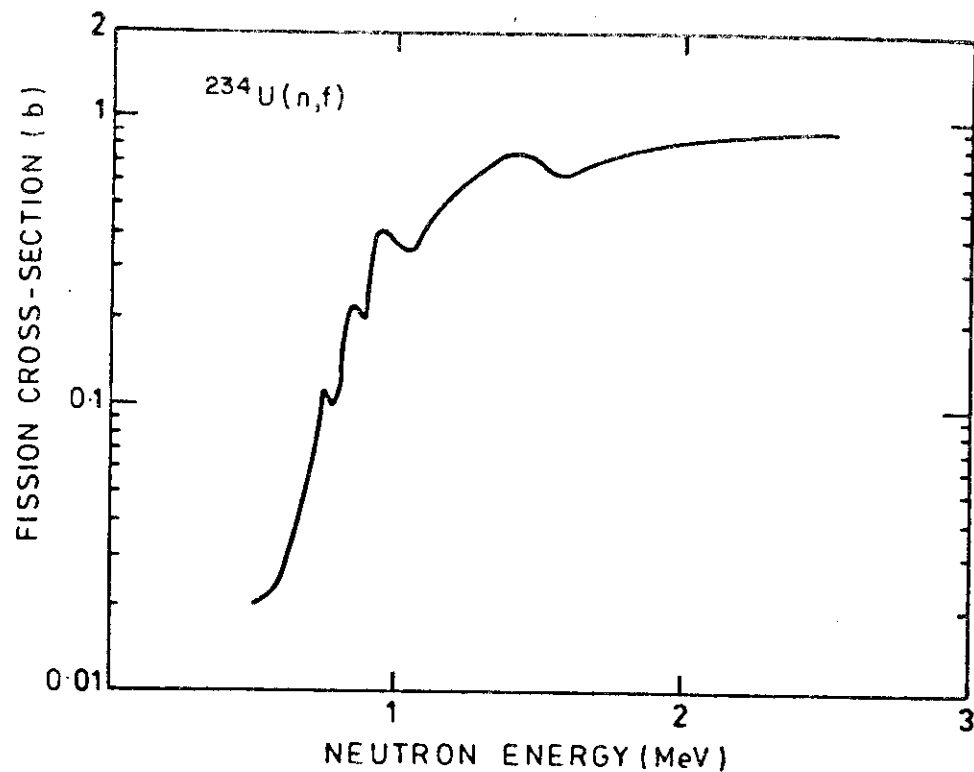


FIG. 4. Neutron fission cross section of ^{234}U . This shows the general feature of a very sharp rise in cross section from sub-barrier energies, which is characteristic of quantal barrier tunneling.

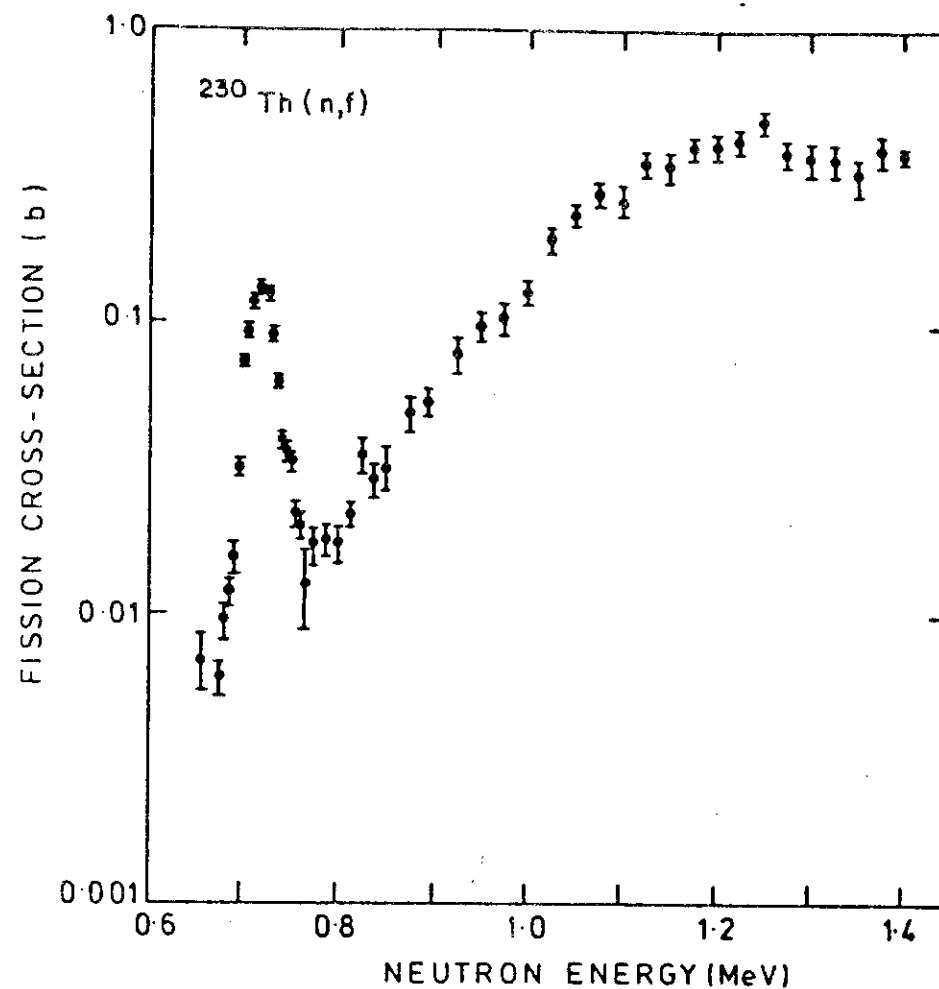


FIG. 6. Neutron fission cross section of ^{230}Th [data of James *et al.* (1972)].

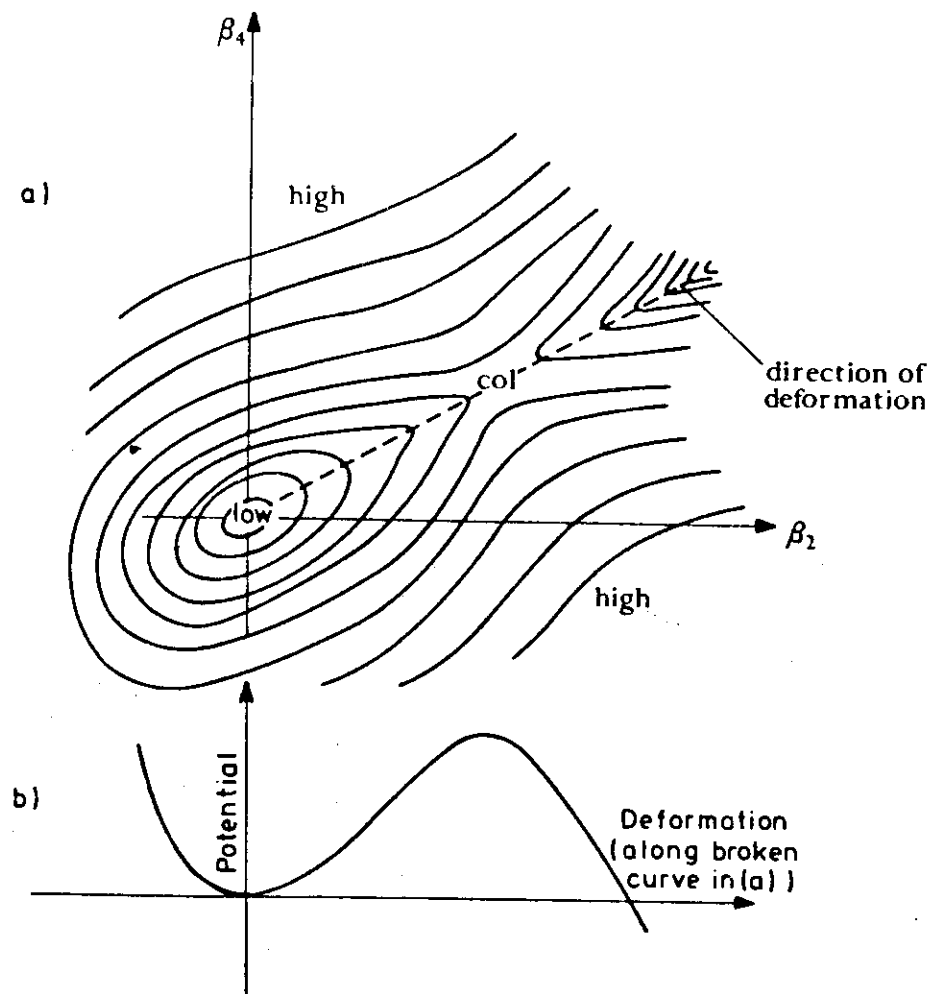


FIG. 1. (a) Schematic diagram of potential energy contours of a fissionable nucleus as a function of the quadrupole and hexadecapole deformation parameters. (b) The potential energy along the minimum energy trajectory for increasing elongation.

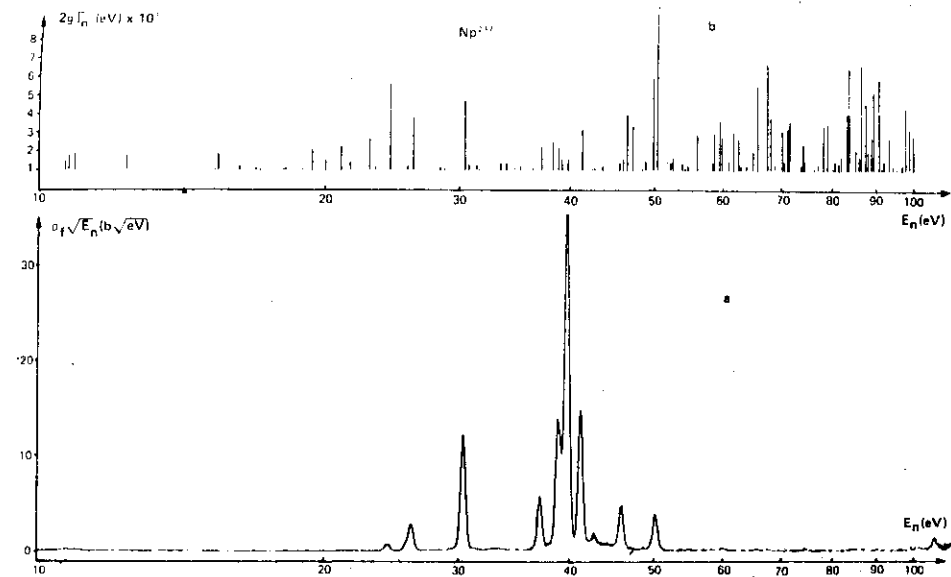


Fig. 45. The Saclay subthreshold fission cross section of ^{237}Np , multiplied by $\sqrt{E_n}$, is plotted as a function of neutron energy E_n , between 10 eV and 100 eV (diagram a). The positions of the resonances as observed in the total cross section, are indicated by bars in diagram b. For each resonance, the height of the bar is proportional to the reduced neutron width $2gI_n^0$ [after A. Michaudon (Nuc 68a)].

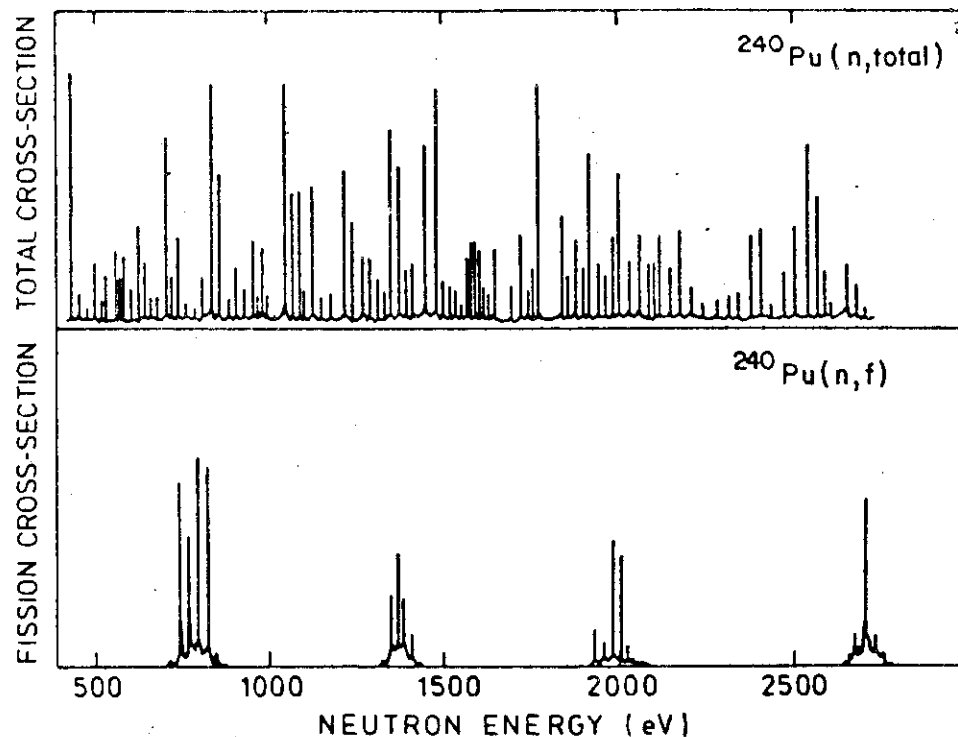


FIG. 7. Above: the total neutron cross section of ^{240}Pu (Kolar and Böckhoff, 1968), showing the large number of fine-structure resonances. Below: the neutron fission cross section of ^{240}Pu (Migneco and Theobald, 1968) showing a very few fine-structure resonances of appreciable strength and those clustered into a few groups that constitute intermediate resonances in the fission channel.

SINGLE HUMP BARRIER

INVERTED PARABOLIC BARRIER

$$T = (1 + \exp [2\pi (V_{\text{MAX}} - E)/\hbar w])^{-1}$$

WKB APPROXIMATIONS

$$T \approx (1 + \exp (2K))^{-1}$$

WHERE

$$K = -I_M \int_{\eta_a}^{\eta_b} d\eta \left[\frac{2B(E - V(\eta))}{\hbar^2} \right]^{1/2}$$

B = MASS PARAMETER

$\eta_{a,b}$ = CLASSICAL TURNING POINTS

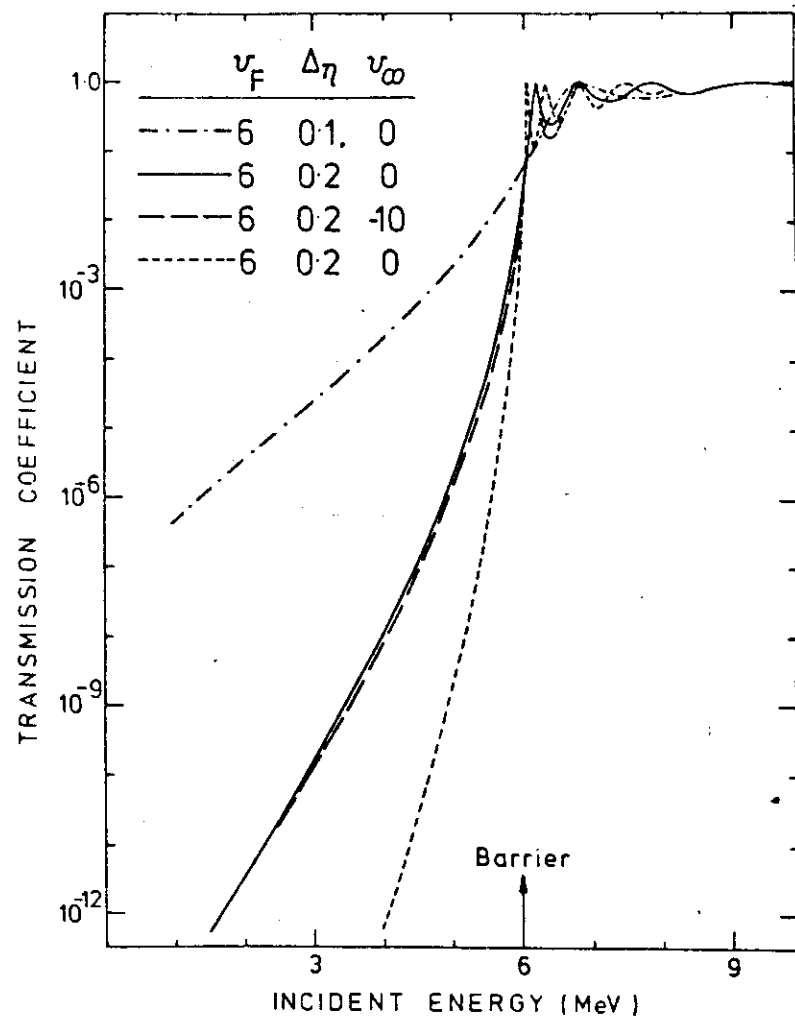


FIG. 26. Transmission coefficient calculated for the passage of a wave through a rectangular barrier (Fig. 25). The inertial parameter is chosen so that $2B/\hbar^2 = 1200 \text{ MeV}^{-1}$ (the deformation parameter η is dimensionless).

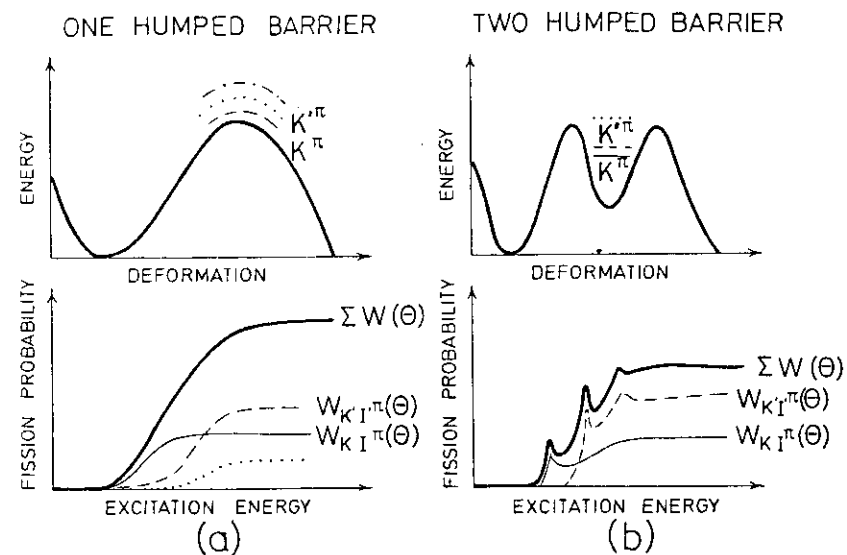


FIG. 152. Near-barrier fission excitation functions. A one-humped barrier gives smoothly rising fission probabilities. Each transition state K^π with its associated rotational band will give a characteristic angular distribution, and the total fission fragment angular distribution can in principle be decomposed into a sum of contributions from each channel K^π . With a two-humped barrier there will be much more structure in the excitation function, which will be dominated by the transition states in the second well and their associated angular distributions.

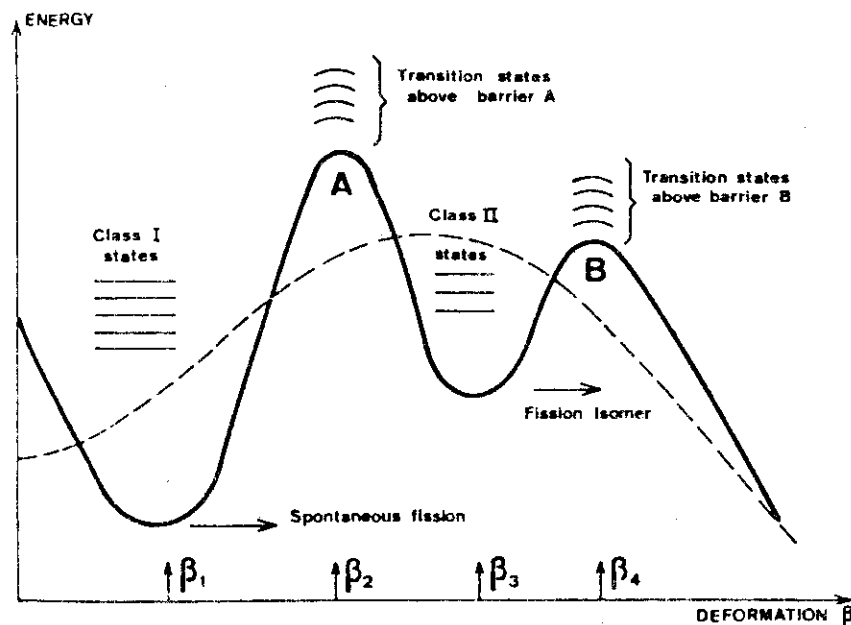


Fig. 65. Fission barrier (solid line) resulting from shell corrections to the LDM barrier (dashed line). As in Fig. 54, the abscissa β gives only an indication of the magnitude of the deformation but does not specify the type of deformation. For certain classes of nuclei, for instance, those having neutron number N in the vicinity of 146, the fission barrier presents two humps A and B, at deformation β_2 and β_1 , respectively, where the shell-energy corrections are positive. These two humps can be separated by a deep second well, at deformation β_3 , where the shell-energy correction is negative. This kind of barrier shape has consequences (discussed in Sect. 5) for the understanding of the fission process.

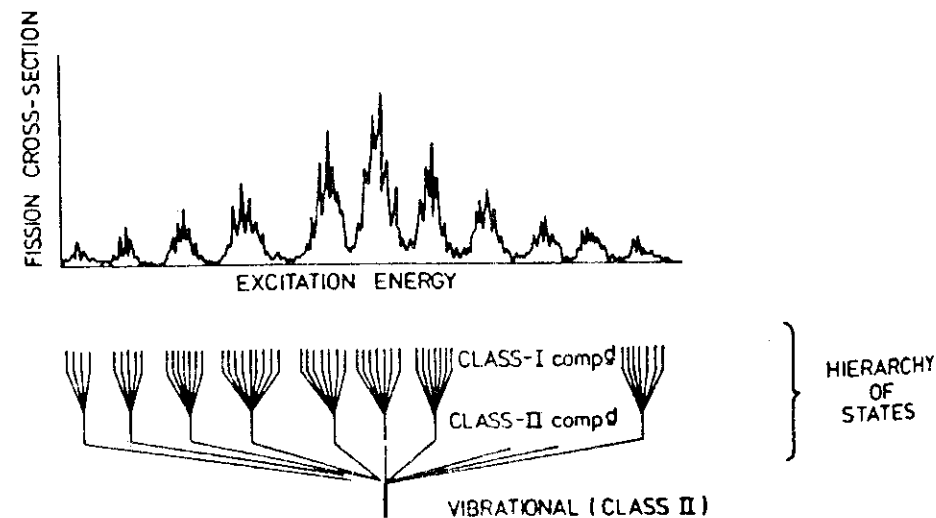


FIG. 95. Schematic illustration of the damping of a vibrational resonance into class-II, and ultimately class-I compound states.

DOUBLE HUMP BARRIER

WKB APPROXIMATION

$$T \approx 1/4 T_A T_B \{ [1/4 (T_A + T_B)]^2 \sin^2 \phi + \cos^2 \phi \}^{-1}$$

WHERE T_A, T_B FROM SINGLE HUMP

ϕ = MATCHING ANGLE

$$T_{\text{MAX}} = \frac{4 T_A T_B}{(T_A + T_B)^2}$$

$$T_{\text{MIN}} = \frac{T_A T_B}{4}$$

UNCOUPLED WKB

$$T \approx \frac{T_A T_B}{(T_A + T_B)}$$

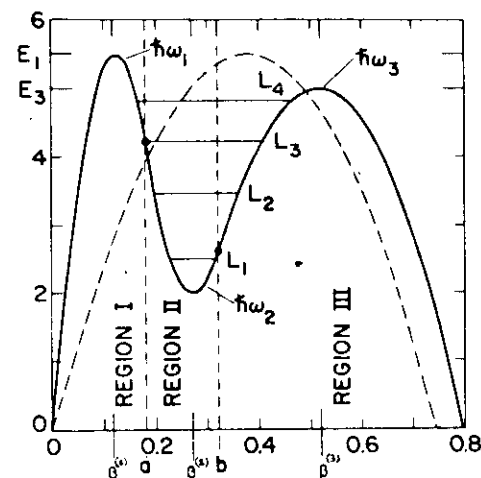


Fig. 75. An illustration of a two-peaked fission barrier parametrized by portions of three smoothly joined parabolas [Eq. (5.21)]. The connecting points a and b define three regions of the potential energy. The locations L_i of the quasi-bound levels are indicated. The dashed curve represents a comparable single-parabolic barrier. Parameters for these two barriers are listed in Table IX [after J. D. Cramer and J. R. Nix (CN 70)].

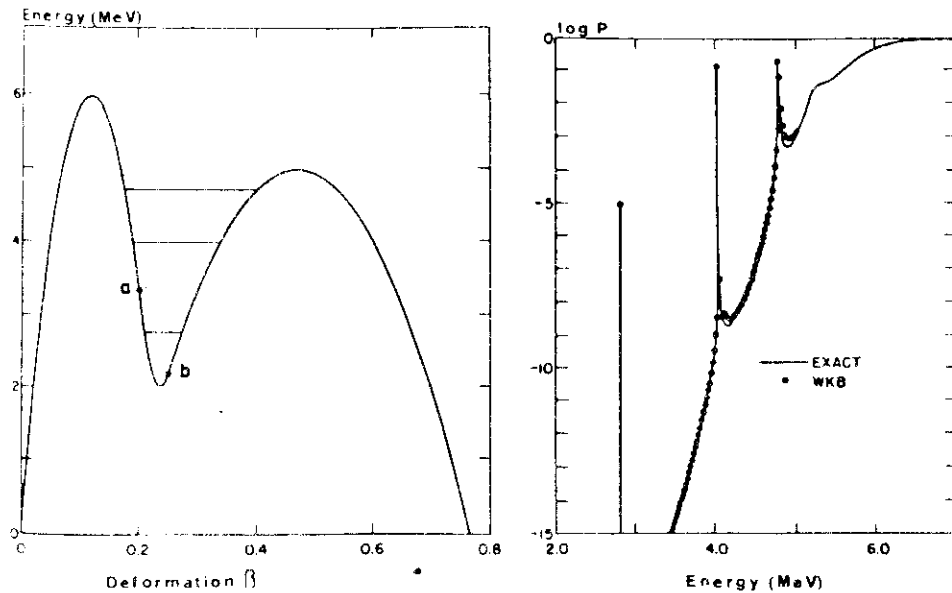


Fig. 76. A comparison of exact and WKB (quasi-classical) penetrabilities for an asymmetric barrier. The potential barrier is shown on the left, with the connecting points *a* and *b* and the positions of the quasi-bound levels indicated. The semilogarithmic plot on the right compares the exact results (solid line) and the WKB results (solid points). The energy shift indicated here at the 4.76 MeV resonance between the WKB and exact methods is 20 keV. The predicted penetrabilities in the valley just above the 4.76 MeV resonance are 1.4×10^{-4} and 5.2×10^{-4} for the WKB and exact methods, respectively. Parameters for this barrier are listed in Table X [after J. D. Cramer and J. R. Nix (CN 70)].

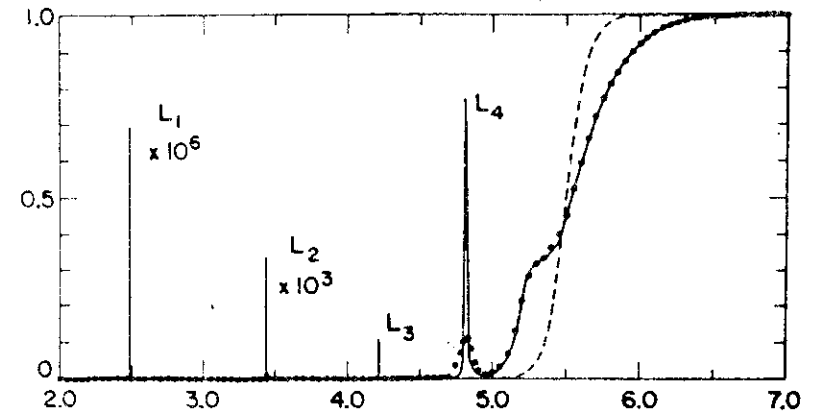


Fig. 74. Linear plot of the penetrability, calculated by the exact method, through the two-peaked barrier of Fig. 75. Note the sharp resonances at the positions of the quasi-bound levels in the intermediate well. To illustrate the influence of experimental resolution, the solid points represent the results of folding the calculated penetrability with a Gaussian function having a full width at half maximum of 100 keV. The dashed curve gives the penetrability for the single-parabolic barrier of Fig. 75 [after J. D. Cramer and J. R. Nix (CN 70)].

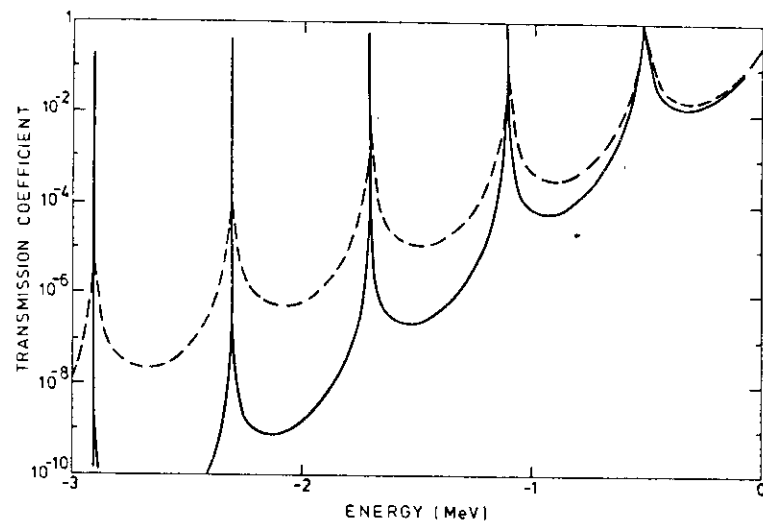


FIG. 34. Schematic picture of the transmission coefficient through a double-humped barrier with damping (represented by an imaginary component in the potential energy) in the secondary well (broken curve) compared with the case of zero damping (full curve). In the first case the imaginary component is 50 keV.

TABLE XII

Summary of Available Fission Data Which Can Provide Information on the Parameters of Double-Humped Fission Barriers*

Fission data	Gives
Spontaneous fission half-life $T_{1/2}^0$	$\frac{E_{fA}}{\hbar\omega_A} + \frac{E_{fB}}{\hbar\omega_B}$ or $\frac{E_f}{\hbar\omega}$
Fission isomers	
a. Spontaneous fission half-life $T_{1/2}^0$	$\frac{E_{fB}}{\hbar\omega_B}$
b. $(x, 2n)$ reaction threshold	E_{II}
c. $\sigma(x, 2n)$ at maximum	E_{fB}
Cross section for near-threshold fission processes, (n, f) and (d, pf)	E_{fA} (or E_{fB}) $\hbar\omega_A$ (or $\hbar\omega_B$) or $\hbar\omega$
Vibrational fission resonances	$\frac{E_{fA}}{\hbar\omega_A}$ and $\frac{E_{fB}}{\hbar\omega_B}$
Intermediate structure	E_{II} $\frac{E_{fA}}{\hbar\omega_A}$ and $\frac{E_{fB}}{\hbar\omega_B}$

* After S. Björnholm (Bio 69b).

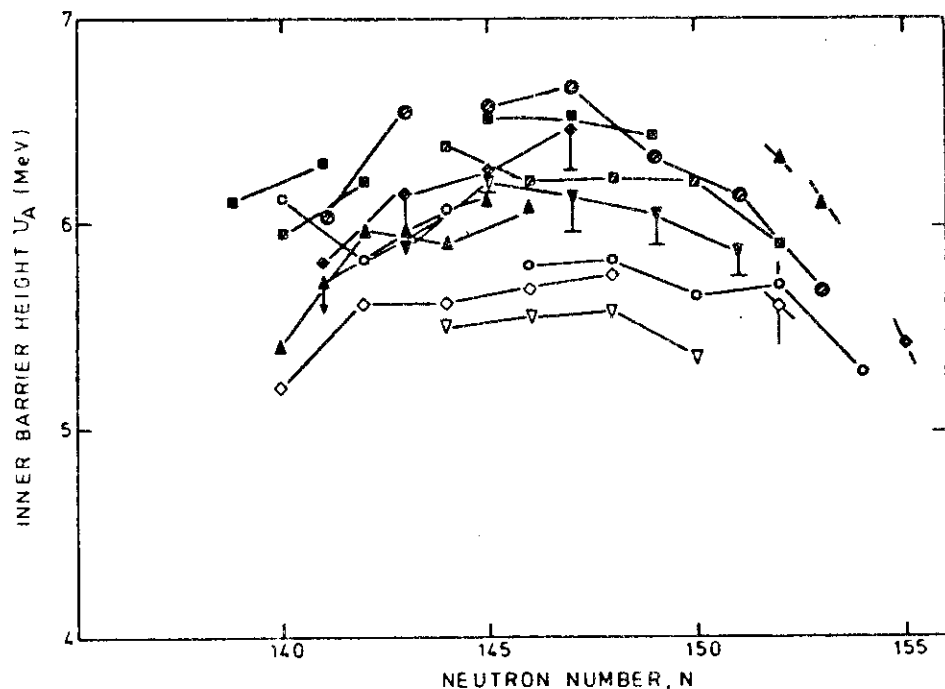


FIG. 132. Inner barrier heights as a function of neutron number. Open symbols denote doubly even nuclides, hatched denote odd-mass, black denote doubly odd, \circ -Th, Cm; \square -Pa, Am; \diamond -U, Cf; \triangle -Np, Bk; ∇ -Pu.

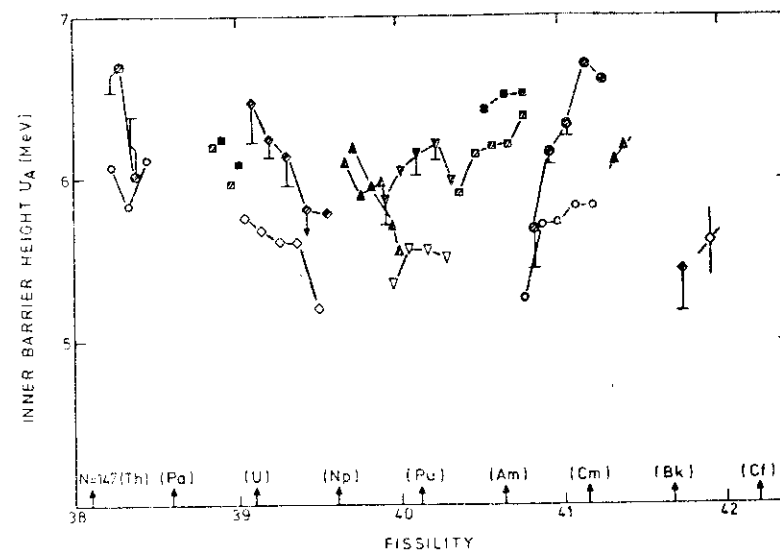


FIG. 133. Inner barrier heights as a function of fissility $Z^2/[A(1 - 1.75(N - Z/A)^2)]$. Vertical arrows on abscissa indicate $N=1$ for various Z . Symbols in Fig. 132.

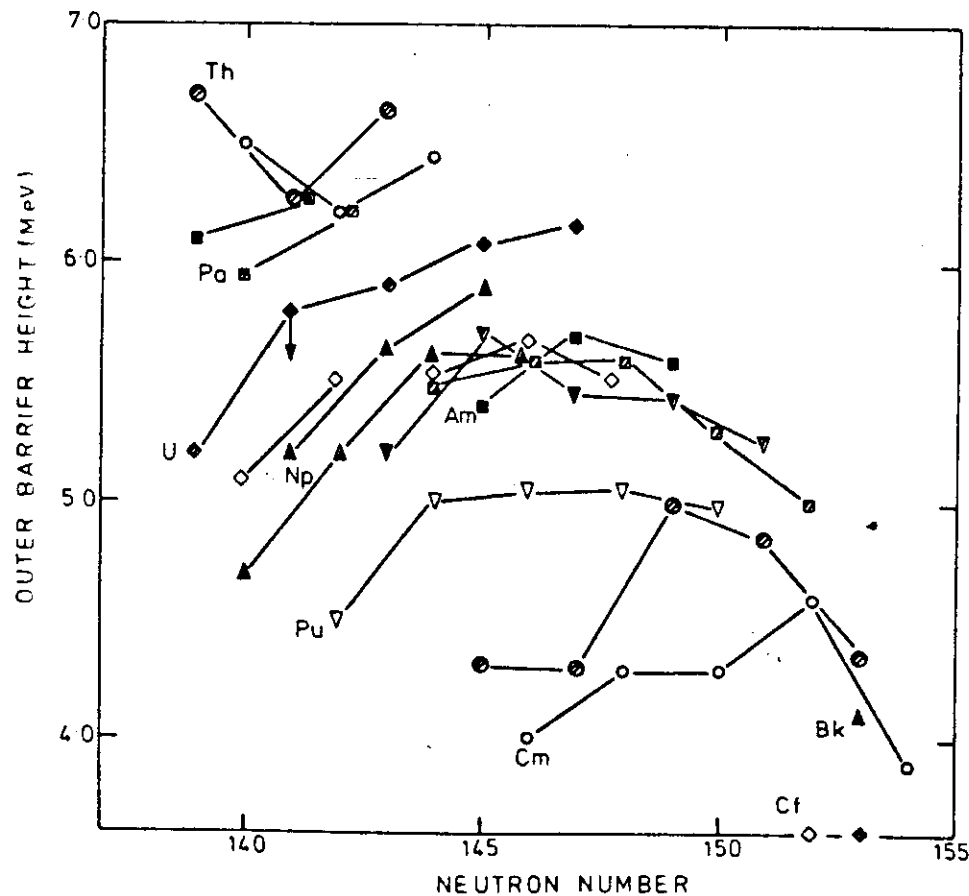


FIG. 134. Outer barrier heights as a function of neutron number. Symbols as in Fig. 132.

23

TABLE XXXI. Recommended values of barrier parameters from analysis of fission cross-section data on the actinide nuclides. It is not claimed that these parameters are unique in the sense of being the only sets that will fit the data. They are designed to be used with the other nuclear parameters given in this section for the purpose of establishing the systematics of actinide fission barrier parameters on a common basis.

Compound nucleus	Neutron separation energy S_n (MeV)	Reactions	Footnote	U_A (MeV)	$\hbar\omega_A$ (MeV)	U_B (MeV)	$\hbar\omega_B$ (MeV)	Comments
^{229}Th	5.23	$^{229}\text{Th}(n, f)$	1			~ 6.7		From value of η_d above 2 MeV
^{230}Th	6.79	$^{230}\text{Th}(n, f)$	2	6.1	1.0	6.5	0.75	See Note 1
^{231}Th	5.13	$^{231}\text{Th}(n, f)$	3, 4					
		$^{230}\text{Th}(n, f)$	5, 6	6.02	0.9	6.27	0.57	Analysis of vibrational resonance structure reported by Yuen <i>et al.</i> (1921). Statistical Hauser-Feshbach analysis gives barriers ~ 0.3 MeV higher. See also Sec. V.
^{232}Th	6.43	$^{232}\text{Th}(n, pf)$	2	5.82	1.0	6.22	0.75	Barrier parameters from pure vibrational model analysis; statistical Hauser-Feshbach calculation with same parameters is about factor 2 too large at high energies.
^{233}Th	4.79	$^{233}\text{Th}(n, f)$	7, 8	6.55	0.8	6.65	0.56	From statistical Hauser-Feshbach calculation. For relation to vibrational structure see Sec. V.
^{234}Th	6.18	$^{234}\text{Th}(n, pf)$	2	6.1	1.0	6.5	0.75	Pure vibrational resonance fit to data. See Fig. 91.
^{235}Pa	5.85	$^{235}\text{Pa}^{\delta}\text{He}(f)$	9	6.1	0.65	6.1	0.45	From statistical Hauser-Feshbach calculation.
^{236}Pa	6.86	$^{236}\text{Pa}^{\delta}\text{He}(df)$	10, 9	5.9	0.8	5.9	0.52	From statistical Hauser-Feshbach calculation.
^{237}Pa	5.57	$^{237}\text{Pa}(n, f)$	11	6.3	0.65	6.25	0.45	Barrier estimates (from Hauser-Feshbach statistical analysis) agree with crude analysis of vibrational resonance structure; see Sec. V.
		$^{236}\text{Pa}(n, pf)$	10					
		$^{235}\text{Pa}^{\delta}\text{He}(f)$	9					
^{238}Pa	6.51	$^{238}\text{Pa}^{\delta}\text{He}(df)$	10, 9	6.2	0.8	6.2	0.52	From statistical Hauser-Feshbach analysis.
^{239}U	5.96	$^{239}\text{U}^{\delta}\text{He}(f)$	9	5.8	0.8	5.2	0.52	From statistical Hauser-Feshbach analysis.
^{240}U	7.28	$^{240}\text{U}^{\delta}\text{He}(df)$	2	5.2	1.04	5.1	0.6	See Note 2.
^{241}U	5.79	$^{241}\text{U}(n, f)$	12, 13	≈ 5.8		≈ 5.8		References cover resonance region, and cross section to 1 keV neutron energy suggests that nuclide is fissile.
								See Note 2.
^{242}U	6.84	$^{242}\text{U}(n, pf)$	14	5.6	1.04	5.5	0.6	
		$^{241}\text{U}(n, f)$	15					
^{243}U	5.31	$^{243}\text{U}(n, f)$	16	6.15	0.8	5.9	0.52	Detailed Hauser-Feshbach calculation with $K' = \frac{1}{2}$ band at barriers 0.2 MeV lower than quoted barrier heights gives better fit than statistical analysis (see Sec. D.2 and Fig. 126). For relation to intermediate structure see Sec. V. C.4 and Sec. VI. D.
^{244}U	6.54	$^{244}\text{U}(n, pf)$	2					See Note 2.
		$^{243}\text{U}(n, pf)$	14					See Note 2.
		$^{242}\text{U}(n, f)$	17	5.63	1.04	5.53	0.6	See Note 3.
^{245}U	5.13	$^{245}\text{U}(n, f)$	18	6.28	0.8	6.08	0.52	From statistical analysis. Detailed Hauser-Feshbach calculation with $K' = \frac{1}{2}$ band 0.1 MeV below these barriers and $\frac{3}{2}$ band 0.1 MeV above gives improved fit (see Sec. VII. D.2).
^{246}U	6.14	$^{246}\text{U}(n, pf)$	2	5.7	1.0	5.7	0.6	See Note 2. Also see Fig. 128 for which calculated photofission cross section has lowest $J'' = 1$ barrier states 0.7 MeV, 0.1 MeV above U_A , U_B , respectively.
		$^{245}\text{U}(n, f)$	19					Resonance data suggest that $K' = 1$ barrier A state could be ~ 1.1 MeV above U_A .
^{247}U	4.86	$^{247}\text{U}(n, f)$	17	6.46	0.8	6.16	0.52	Reference cross section for barrier level density parameters of odd-A nuclides (see Sec. VII. C.2). For relation to intermediate structure see Sec. VI.

24

TABLE XXXI. (Continued.)

Compound nucleus	Neutron separation energy S_n (MeV)	Reactions	Footnote	U_A (MeV)	h_{wA} (MeV)	U_B (MeV)	h_{wB} (MeV)	Comments
^{245}U	5.92	$^{238}\text{U}(t, pf)$	2	5.75	1.04	5.5	0.6	See Note 2.
^{235}Np	7.35	$^{232}\text{U}(^3\text{He}, tf)$	9	5.4	0.8	4.7	0.52	From statistical Hauser-Feshbach analysis.
^{234}Np	6.12	$^{231}\text{U}(^3\text{He}, dt)$	10	5.7	0.65	5.2	0.45	From statistical Hauser-Feshbach analysis.
^{235}Np	6.39	$^{234}\text{U}(^3\text{He}, tt)$ $^{234}\text{U}(^3\text{He}, dt)$	9 10	6.0	0.8	5.2	0.52	From statistical Hauser-Feshbach analysis.
^{236}Np	5.69	$^{235}\text{U}(^3\text{He}, ff)$ $^{235}\text{U}(^3\text{He}, dt)$	9 10, 9	5.9	0.65	5.7	0.45	From statistical Hauser-Feshbach analysis.
^{237}Np	6.59	$^{236}\text{U}(^3\text{He}, tt)$ $^{236}\text{U}(^3\text{He}, dt)$	9 10, 9	5.9	0.8	5.6	0.52	From statistical Hauser-Feshbach analysis.
^{238}Np	5.49	$^{237}\text{Np}(t, pf)$	10	6.2	0.65	5.9	0.45	From statistical and detailed Hauser-Feshbach analysis.
^{239}Np	6.25	$^{238}\text{U}(^3\text{He}, tt)$ $^{238}\text{U}(^3\text{He}, f)$	9 20, 21, 17					For relation to intermediate structure see Sec. VI.
^{239}Pu	5.9	$^{237}\text{Np}(^3\text{He}, t)$	9	5.9	0.8	5.2	0.52	From statistical Hauser-Feshbach analysis.
^{240}Pu	7.0	$^{239}\text{Pu}(^3\text{He}, df)$	2	5.5	1.04	5.0	0.6	See Note 2.
^{241}Pu	5.66	$^{240}\text{Pu}(n, f)$	22	6.3	0.8	5.7	0.52	From statistical Hauser-Feshbach analysis. Detailed Hauser-Feshbach calculations give good fit with $K^{\pi} = \frac{1}{2}^+, \frac{3}{2}^+, \frac{5}{2}^+$ bands of barrier states ~ 0.15 MeV below quoted barriers. For relation to intermediate structure see Sec. VI.
^{240}Pu	6.52	$^{238}\text{Pu}(t, p^+)$	2	5.57	1.04	5.07	0.6	See Notes 2 and 3 and Fig. 129. Relation to intermediate structure described in Secs. V and VI.
^{241}Pu	5.24	$^{239}\text{Pu}(n, f)$ $^{240}\text{Pu}(n, f)$	17 23, 24, 25 10	6.1	0.8	5.5	0.52	See comment under ^{239}Pu .
^{242}Pu	6.30	$^{241}\text{Pu}(t, pf)$ $^{241}\text{Pu}(n, f)$	2 26, 27, 28	5.6	1.04	5.1	0.6	See Note 2 and Fig. 131. Detailed Hauser-Feshbach analysis.
^{243}Pu	5.04	$^{242}\text{Pu}(n, f)$	29, 30	6.0	0.8	5.4	0.52	From statistical Hauser-Feshbach analysis. For relation to intermediate structure see Sec. VI.
^{244}Pu	5.02	$^{243}\text{Pu}(t, pf)$	2	5.4	1.04	5.0	0.6	See Note 2.
^{245}Pu	4.76	$^{244}\text{Pu}(n, f)$	30	5.8	0.8	5.3	0.52	From statistical Hauser-Feshbach analysis. Detailed Hauser-Feshbach calculation suggests lowest barrier states (perhaps $K^{\pi} = \frac{1}{2}^+, \frac{3}{2}^+, \frac{5}{2}^+$) are ~ 0.1 MeV lower than Bars.
^{238}Am	7.25	$^{235}\text{Pu}(^3\text{He}, tf)$	9	5.4	0.8	5.6	0.52	From statistical Hauser-Feshbach analysis.
^{240}Am	5.94	$^{238}\text{Pu}(^3\text{He}, df)$	10	6.5	0.65	5.4	0.45	From statistical Hauser-Feshbach analysis.
^{241}Am	6.66	$^{240}\text{Pu}(^3\text{He}, tt)$ $^{240}\text{Pu}(^3\text{He}, df)$	9 10	6.2	0.8	5.7	0.52	From statistical Hauser-Feshbach analysis.
^{242}Am	5.54	$^{241}\text{Am}(d, pf)$	10	6.5	0.65	5.7	0.45	From statistical and detailed (on n, f) Hauser-Feshbach analysis.
^{243}Am	6.43	$^{242}\text{Am}(t, pf)$ $^{241}\text{Am}(n, f)$ $^{242}\text{Pu}(^3\text{He}, df)$	9 31, 32 10, 9	6.2	0.8	5.6	0.52	See Note 4. From statistical Hauser-Feshbach analysis.
^{244}Am	5.37	$^{243}\text{Am}(d, pf)$	14	6.4	0.65	5.6	0.45	From statistical and detailed (on n, f) Hauser-Feshbach analysis.

25

TABLE XXXI. (Continued.)

Compound nucleus	Neutron separation energy S_n (MeV)	Reactions	Footnote	U_A (MeV)	h_{wA} (MeV)	U_B (MeV)	h_{wB} (MeV)	Comments
^{245}Am	6.05	$^{243}\text{Am}(t, f)$ $^{243}\text{Am}(t, pf)$	33, 27 10	6.2	0.8	5.3	0.52	From statistical Hauser-Feshbach analysis.
^{247}Am	5.86	$^{245}\text{Cm}(t, of)$	10	5.8	0.8	5.0	0.52	From statistical Hauser-Feshbach analysis.
^{248}Cm	6.1	$^{247}\text{Am}(^3\text{He}, tf)$	9	6.6	0.8	4.3	0.52	From statistical Hauser-Feshbach analysis.
^{249}Cm	6.9	$^{248}\text{Am}(^3\text{He}, df)$	9	5.8	1.04	4.0	0.6	From statistical Hauser-Feshbach analysis.
^{250}Cm	5.6	$^{249}\text{Am}(^3\text{He}, tf)$	9	6.7	0.8	4.3	0.52	From statistical Hauser-Feshbach analysis.
^{251}Cm	6.8	$^{250}\text{Am}(^3\text{He}, df)$	2, 9	5.8	1.04	4.3	0.6	From statistical Hauser-Feshbach analysis.
^{252}Cm	5.52	$^{251}\text{Cm}(n, f)$	33	6.3	0.8	5.0	0.52	From statistical Hauser-Feshbach analysis.
^{253}Cm	6.43	$^{252}\text{Cm}(t, f)$	33	5.7	1.04	4.3	0.6	From statistical Hauser-Feshbach analysis.
^{254}Cm	5.16	$^{253}\text{Cm}(n, f)$	33	6.2	0.8	4.8	0.52	From statistical Hauser-Feshbach analysis (and see Note 5).
^{255}Cm	6.21	$^{254}\text{Cm}(n, p, f)$	2	5.7	1.04	4.6	0.6	From statistical Hauser-Feshbach analysis.
^{256}Cm	4.71	$^{255}\text{Cm}(n, f)$	33	5.7	0.8	4.3	0.52	From statistical Hauser-Feshbach analysis (and see Note 6).
^{257}Cm		$^{256}\text{Cm}(n, pf)$	2	5.3	1.04	3.9	0.6	From statistical Hauser-Feshbach analysis.
^{258}Bk	6.21	$^{256}\text{Cm}(^3\text{He}, df)$	10	6.2	0.8			From statistical Hauser-Feshbach analysis.
^{259}Bk	4.97	$^{258}\text{Bk}(n, f)$	34	6.1	0.85	4.1	0.45	From statistical Hauser-Feshbach analysis.
^{260}Cf	6.62	$^{259}\text{Cf}(n, f)$	35, 36	5.6	1.04	3.6	0.6	From statistical Hauser-Feshbach analysis.
^{261}Cf	4.83	$^{260}\text{Cf}(n, f)$	37	5.4	0.8	3.6	0.52	See Note 7.

Note 1. The (t, of) data can be fitted by these parameters using a *prolate vibrational* model built on a $K^{\pi} = 0^+$ rotational band over the barriers and making some allowance for the presence of a $K^{\pi} = 0^+$ band. The data cannot be fitted by a strong damping model with the same barrier heights and h_{wB} reduced to 0.6 MeV. The fission cross section data are adequately fitted by specific calculations using these barrier heights with rotational bands at the following positions (energy units in MeV)

	Barrier A	Barrier B
K^{π}	$E_A - S_n$	$E_B - S_n$
0^+	~ 0.9	~ 0.25
2^+	~ 0.53	~ 0.5
1^+	~ 0.22	~ 0.75
2^-	~ 1.0	~ 0.8

statistical calculations in the region of 1 MeV are almost a factor of 2 too high; this tends to be a common feature of the statistical calculations on *Tl* nuclei suggesting that barrier B densities might be overestimated (but see Sec. VII.D.3). Resonance region data give fission widths ranging from 4 meV to >160 meV and resonance spacing of 0.41 eV; this is consistent with position of $J^{\pi} = 3^+$ barrier state implied above (giving $\Gamma(3^+) \approx 10$ meV).

26

TABLE XXXI. (Continued.)

Note 2. Barrier parameters fit a calculation of fission probability through the $K^{\pi}=0^{+}$ rotational band across the barrier. A damped vibrational model has been assumed and the calculation includes the effect of Porter-Thomas fluctuations in the class-II levels. Porter-Thomas fluctuations in the class-I levels have not been included but neither has experimental resolution and these two effects tend to be compensatory.

Note 3. The statistical model calculations of fission cross-sections of ^{235}U and ^{239}Pu have been adjusted simultaneously to give the barrier densities that have been used for statistical calculations on other even compound nuclei (see Sec. VII.C.2).

Note 4. Analysis of spontaneous fission isomerism suggests $\nu_B \sim 5.6$ MeV. Resonance data at low neutron energies give $\Gamma_{\psi} \sim 0.18$ MeV. This agrees with barrier parameters given.

Note 5. Parameters are from statistical model fit. Specific calculation employs $J^{\pi}=3/2^{+}$ barrier states 0.05 MeV below the statistical parameters, $J^{\pi}=1/2^{+}$ 0.05 MeV above, $1/2^{+}$ 0.08 MeV above.

Note 6. Parameters are from statistical model fit. Specific calculation employs $J^{\pi}=7/2^{+}$, $9/2^{+}$ barrier states 0.2 MeV below the statistical parameters, $J^{\pi}=1/2^{+}$ 0.05 MeV above.

Note 7. Parameters are from statistical model fit. Specific calculation has $J^{\pi}=3/2^{+}$, $5/2^{+}$ barrier states 0.25 MeV below statistical values, $3/2^{+}$, 0.18 MeV below. Resonance data indicate fission widths are of the order of magnitude to be explained by barrier parameters.

TABLE XXXII. Summary of barrier and ground-state energies. All energies are in MeV. Most of the numbers are taken from Tables V-VII and XXXI, subtracting a small correction for odd- A nuclei; see text. The ^{223}Ra barriers are from Weber *et al.* (1976), and the ^{223}Ac , ^{227}Th , ^{228}Th , ^{232}Pu , and ^{234}Pu barrier values are due to Habs (1977). The energy E_1 relative to the spherical shape of the liquid drop is based on Myers and Swiatecki (1967) with experimental masses from Wapstra and Gove (1971). Those relative to the droplet are from Myers (1977) with experimental masses from Wapstra and Bos (1977).

Isotope	U_A	E_{II} (Relative to ground state)	U_B	E_1 Rel. to spherical: liq. drop	droplet
^{223}Ra	8.0 ± 0.5		5.5 ± 0.5	0.92	0.16
^{223}Ac	6.0 ± 0.8		7.7 ± 0.3	0.23	-0.95
^{227}Th	5.9 ± 0.3		6.6 ± 0.3	0.32	-0.94
^{228}Th	6.2 ± 0.3		6.5 ± 0.3	0.20	-0.95
^{229}Th			6.5 ± 0.3	0.37	-0.83
^{230}Th	6.1 ± 0.2		6.5 ± 0.3	0.33	-0.75
^{231}Th	6.0 ± 0.1	< 5.8	6.1 ± 0.3	0.39	-0.73
^{232}Th	5.8 ± 0.2	< 4.5	6.2 ± 0.2	0.44	-0.54
^{233}Th	6.3 ± 0.2	< 6.2	6.3 ± 0.2	0.57	-0.40
^{234}Th	6.1 ± 0.2		6.5 ± 0.2	0.63	-0.19
^{235}Pa	5.9 ± 0.2		5.9 ± 0.3	0.26	-1.03
^{236}Pa	6.1 ± 0.3	< 5.7	6.2 ± 0.2	0.09	-1.16
^{237}Pa	6.1 ± 0.3		6.1 ± 0.3	0.26	-0.95
^{238}U	5.2 ± 0.2		5.1 ± 0.3	-0.19	-1.52
^{239}U	5.5 ± 0.2		5.5 ± 0.2	-0.28	-1.58
^{240}U	5.9 ± 0.2	2.5 ± 0.3	5.6 ± 0.2	-0.26	-1.59
^{241}U	5.6 ± 0.2	2.3 ± 0.2	5.5 ± 0.2	-0.15	-1.38
^{242}U	6.1 ± 0.2	2.5 ± 0.4	5.9 ± 0.2	-0.20	-1.43
^{243}U	5.7 ± 0.2	2.6 ± 0.01	5.7 ± 0.2	0.05	-1.04
^{244}U	6.3 ± 0.2	1.9 ± 0.3	6.1 ± 0.2	0.10	-1.00
^{245}U	5.7 ± 0.2		5.5 ± 0.2	0.31	-0.63
^{246}Np	5.5 ± 0.2		5.1 ± 0.2	-0.63	-2.06
^{247}Np	5.5 ± 0.2		5.2 ± 0.2	-0.51	-1.96
^{248}Np	5.8 ± 0.2		5.6 ± 0.2	-0.65	-2.08
^{249}Np	5.7 ± 0.2	2.8 ± 0.3	5.4 ± 0.2	-0.43	-1.85
^{250}Np	6.1 ± 0.2	2.3 ± 0.3	6.0 ± 0.2	-0.61	-1.98
^{251}Np	5.9 ± 0.2		5.4 ± 0.2	-0.25	-1.58
^{252}Pu	5.3 ± 0.4			-0.16	-1.50
^{254}Pu	5.8 ± 0.7			-0.50	-1.89
^{255}Pu		2.6 ± 0.4	5.1 ± 0.4	-0.71	-2.22
^{256}Pu			4.5 ± 0.4	-0.76	-2.23
^{257}Pu		2.8 ± 0.2		-0.86	-2.41
^{258}Pu	5.5 ± 0.2	2.7 ± 0.2	5.0 ± 0.2	-0.81	-2.29
^{259}Pu	6.2 ± 0.2	2.6 ± 0.2	5.5 ± 0.2	-0.98	-2.50
^{260}Pu	5.6 ± 0.2	2.4 ± 0.3	5.1 ± 0.2	-0.71	-2.15
^{261}Pu	6.1 ± 0.2	1.9 ± 0.3	5.4 ± 0.2	-0.70	-2.17
^{262}Pu	5.6 ± 0.2		5.1 ± 0.2	-0.46	-1.81
^{263}Pu	5.9 ± 0.2	1.7 ± 0.3	5.2 ± 0.2	-0.48	-1.84
^{264}Pu	5.4 ± 0.2		5.0 ± 0.2	-0.21	-1.43
^{265}Pu	5.6 ± 0.2		5.0 ± 0.2	-0.15	-1.37
^{237}Am		2.4 ± 0.2		(-1.0)	-2.54
^{238}Am		2.6 ± 0.2		-1.32	-2.83
^{239}Am	6.2 ± 0.3	2.4 ± 0.2		-1.15	-2.76
^{240}Am	6.5 ± 0.2	3.0 ± 0.2	5.2 ± 0.3	(-1.40)	-2.99
^{241}Am	6.0 ± 0.2	2.2 ± 0.2	5.1 ± 0.3	-1.05	-2.67
^{242}Am	6.5 ± 0.2	2.9 ± 0.2	5.4 ± 0.3	-1.14	-2.71
^{243}Am	5.9 ± 0.2	2.3 ± 0.2	5.4 ± 0.3	-0.76	-2.33
^{244}Am	6.3 ± 0.2	2.8 ± 0.4	5.4 ± 0.3	-0.91	-2.42
^{245}Am	5.9 ± 0.2		5.2 ± 0.3	-0.48	-1.95
^{247}Am	5.5 ± 0.2			(-0.13)	-1.49
^{241}Cm	6.3 ± 0.3	2.1 ± 0.3	4.3 ± 0.5	-1.57	-3.25
^{242}Cm	5.8 ± 0.4		4.0 ± 0.5	-1.35	-2.96
^{243}Cm	6.4 ± 0.3	1.9 ± 0.3		-1.41	-3.08
^{244}Cm	5.8 ± 0.2		4.3 ± 0.3	-1.26	-2.87
^{245}Cm	6.2 ± 0.2	2.1 ± 0.3		-1.37	-3.03
^{246}Cm	5.7 ± 0.2		4.2 ± 0.3	-1.13	-2.69
^{247}Cm	6.0 ± 0.2			-1.10	-2.70
^{248}Cm	5.7 ± 0.2			-0.86	-2.35
^{249}Cm	5.6 ± 0.2			-0.63	-2.13

BARRIER HEIGHT

INNER

$$V \text{ (EVEN)} \approx 5.7 - 0.01067 * (N-147)^2 \text{ MeV}$$

$$\text{(ODD-A)} \approx 6.3 - 0.01067 * (N-147)^2$$

$$\text{(ODD)} \approx 6.5 - 0.01067 * (N-147)^2$$

LEVEL DENSITIES

LEVEL DENSITY IS INCREASED AT

$$\rho_A \approx 4 * \rho$$

INNER BARRIER

$$\rho_B \approx 2 * \rho$$

OUTER BARRIER

FOUND BY EFFECT ON NEUTRON COMPETITIONS.

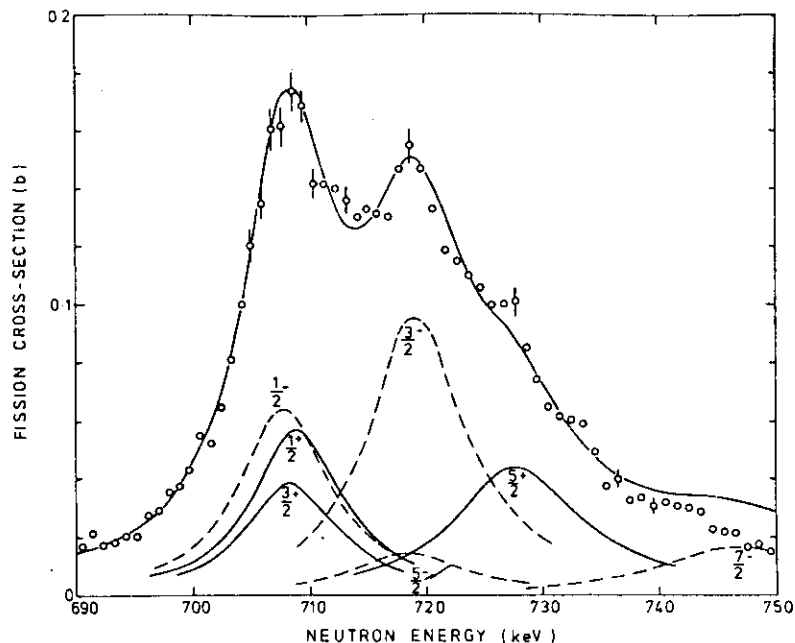


FIG. 166. High resolution data on the neutron fission cross section of ^{236}Th (Blons *et al.*, 1980) and attempted fit with the model of Boldemann *et al.* (1980) based on near-degeneracy of $K^\pi = \frac{1}{2}^-$ and $\frac{3}{2}^-$ rotational bands. Cross-section components for individual spin and parity combinations J^π are also shown.

31

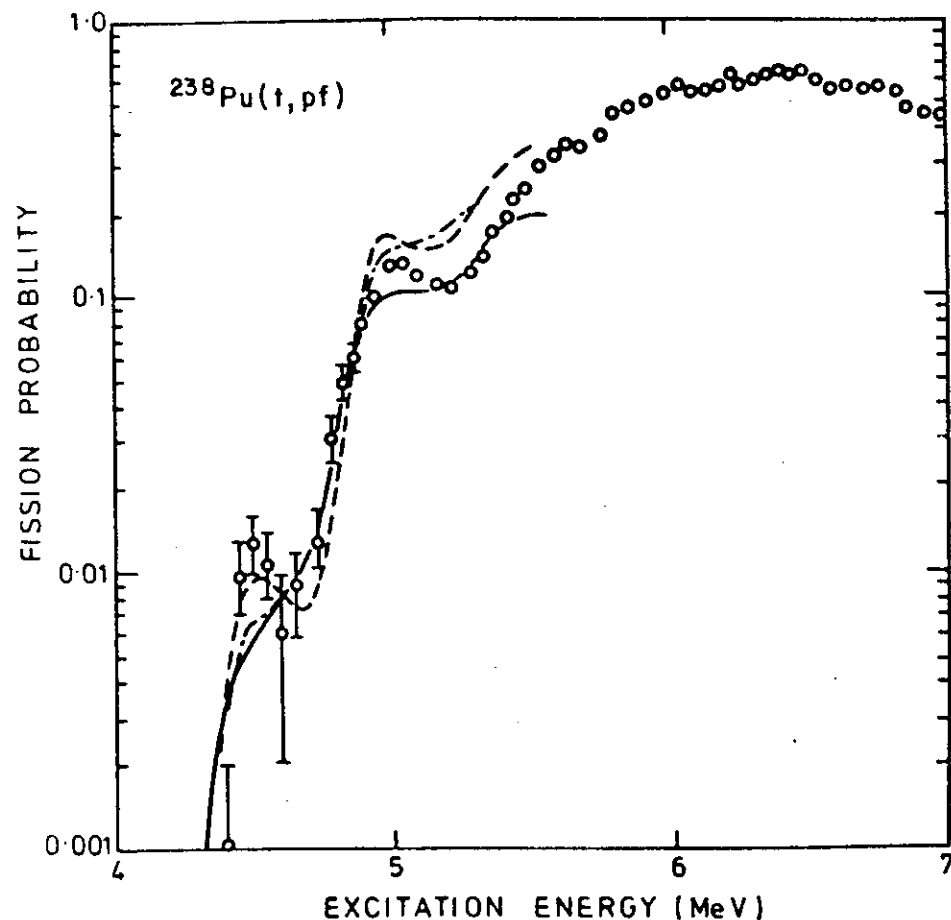


FIG. 129. The fission probability of ^{240}Pu as measured in the (t, pf) reaction (Back *et al.*, 1974a). The full curve assumes the parameters $U_A = 5.55$ MeV, $U_B = 5.05$ MeV, $\Gamma_{v(D)} = 0.2$ MeV, and a simple $K^\pi = 0^+$ rotational band of transition states at the inner barrier. The short dashed and dot-dashed curves assume a more complex spectrum of transition states, appropriate to axial asymmetry, at the inner barrier. Their parameters are otherwise the same with $\Gamma_{v_{II}(D)} = 0.2$ MeV for the dot-dashed curve, $\Gamma_{v_{II}(D)} = 0.1$ MeV for the short dashed curve.

32

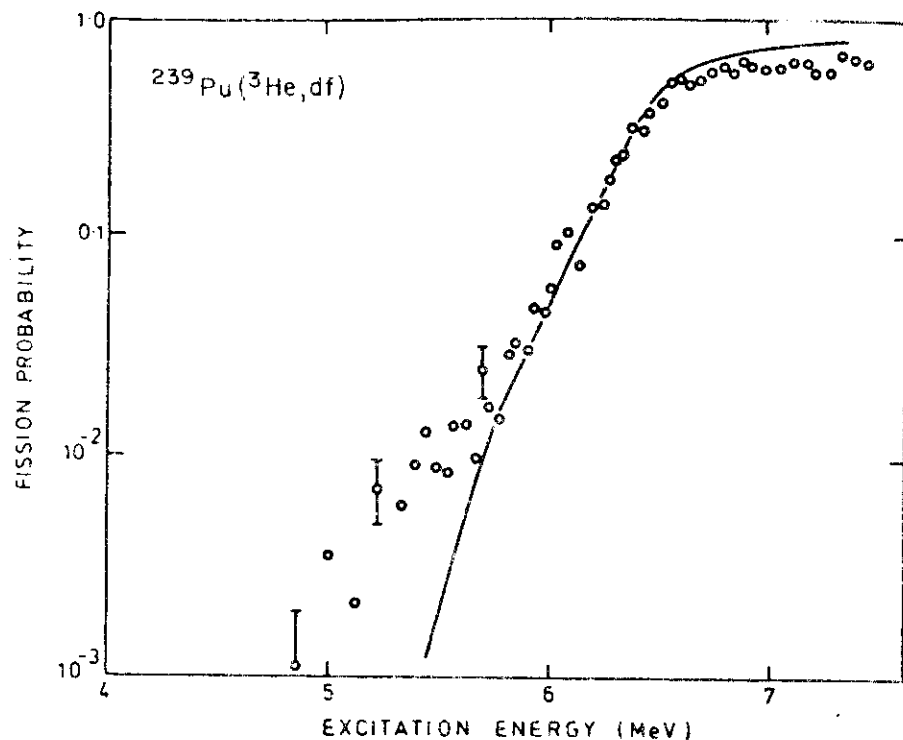


FIG. 127. The fission probability of ^{240}Am . Data and calculation on $^{239}\text{Pu}(^3\text{He}, df)$ reaction. The data are from Back *et al.* (1974c).

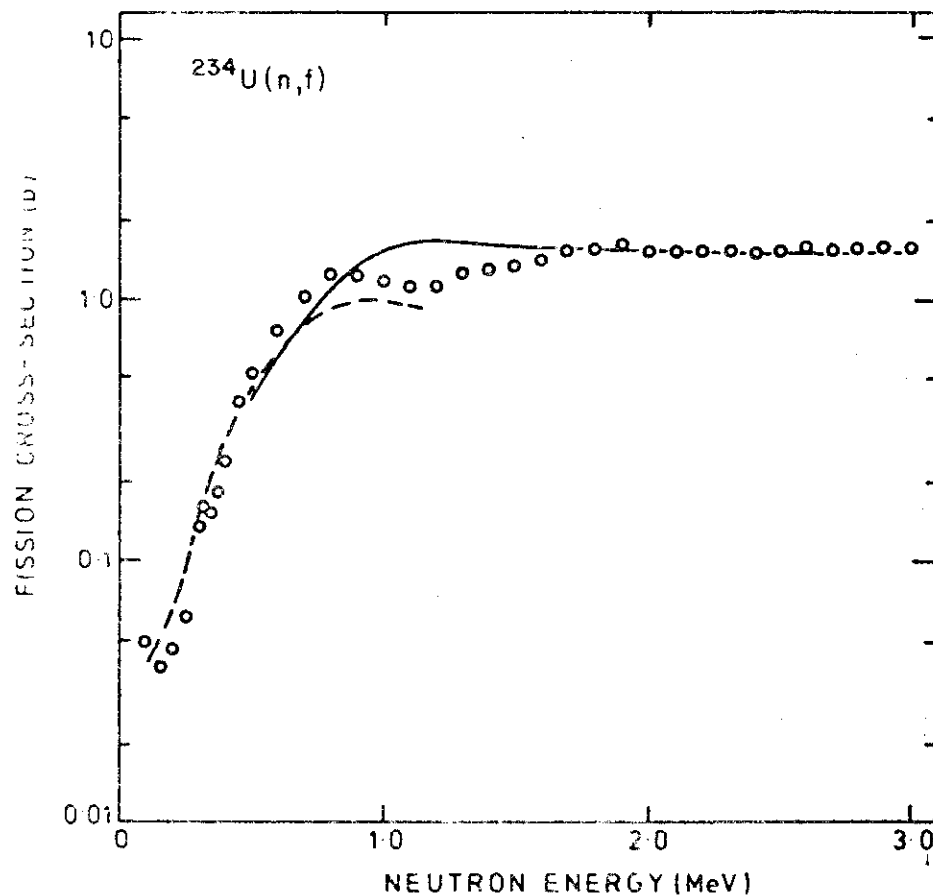


FIG. 126. Neutron fission cross section of ^{234}U (--- detailed Hauser-Feshbach calculation with barrier states $K^\pi = \frac{1}{2}^+$ band at 5.96 MeV (barrier A), 5.71 MeV (B), $K^\pi = \frac{3}{2}^+$ band at 6.36 MeV (A), 6.11 MeV (B) plus continuum, — statistical Hauser-Feshbach calculation.

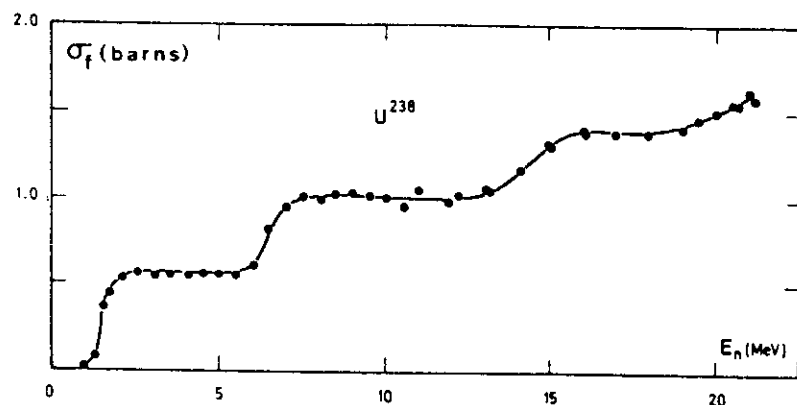


Fig. 5. Neutron-induced fission cross section of ^{238}U plotted as a function of neutron energy E_n (SHN 58). The general behavior of the fission cross section illustrates the sharp rises which occur at thresholds for first chance fission ($E_n \sim 1.5$ MeV), second chance fission ($E_n \sim 6.5$ MeV), etc. This cross section is not meant to show structures which actually appear in more accurate data (see Fig. 78).

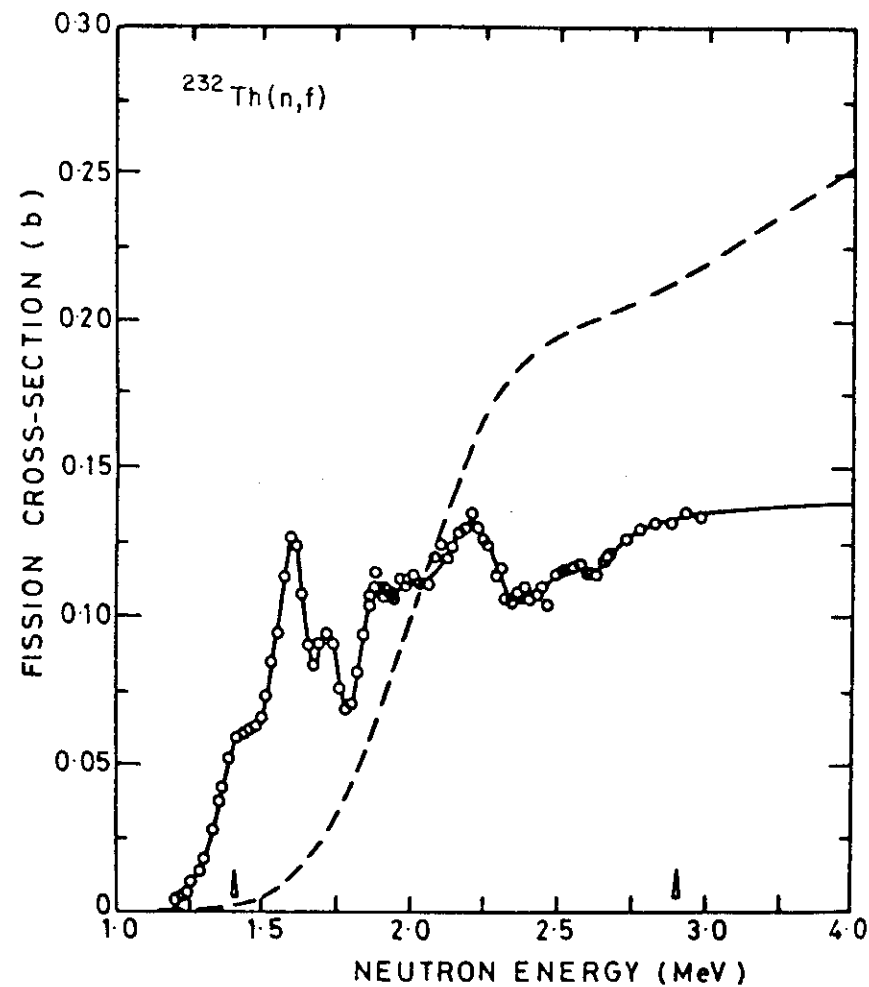


FIG. 136. The calculated neutron fission cross section of ^{232}Th up to 4 MeV, as based on the double-humped barrier parameters of Table XXXI, compared with data (circles and full curve).

TABLE II
FISSION PARAMETERS FOR $n + {}^{239}\text{Pu}$ CALCULATIONS^a

		Barrier Height (MeV)	h_0 (MeV)	Density Enhancement
${}^{240}\text{Pu}$	A	5.8	0.8	16
	B	5.45	0.6	2
${}^{239}\text{Pu}$	A	5.7	0.60	2.5
	B	5.05	0.50	2.5
${}^{238}\text{Pu}$	A	6.1	0.9	5
	B	5.55	0.85	2

^aThe isotopes appearing in the table are compound nuclei populated in the multichance fission of $n + {}^{239}\text{Pu}$. The inner and outer fission barriers are labeled A and B, respectively. The density enhancements shown are multiplied by $U^{1/4}$ (where U is excitation energy, $U > 1$) to obtain overall level density enhancements.

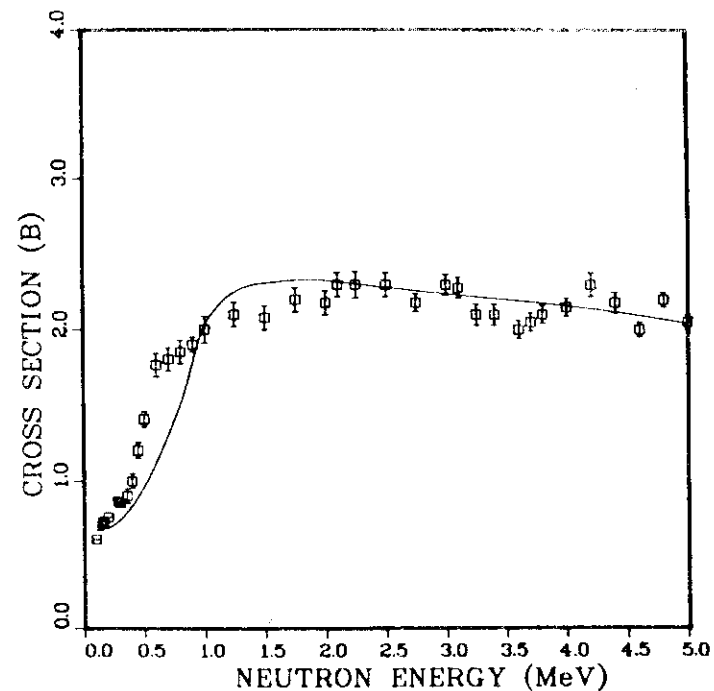


Fig. 4. Calculated ${}^{238}\text{Pu}(n,f)$ cross sections used to obtain initial values for the ${}^{239}\text{Pu}$ barrier parameters appearing in Table II are compared with the data of Budtz-Jørgensen et al.²⁸

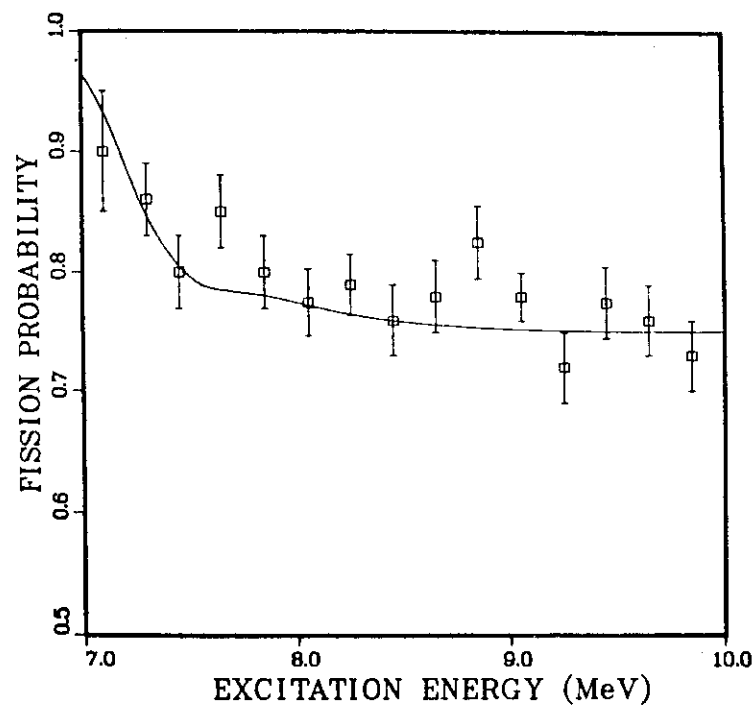


Fig. 5. Comparison of our fits with fission probabilities measured in the $^{237}\text{Np}(^3\text{He},d)^{238}\text{Pu}(f)$ reaction. In these fits, which were used to determine the ^{238}Pu barrier parameters of Table II, explicit account was taken of the compound-nucleus spin populations produced in this direct reaction.

39

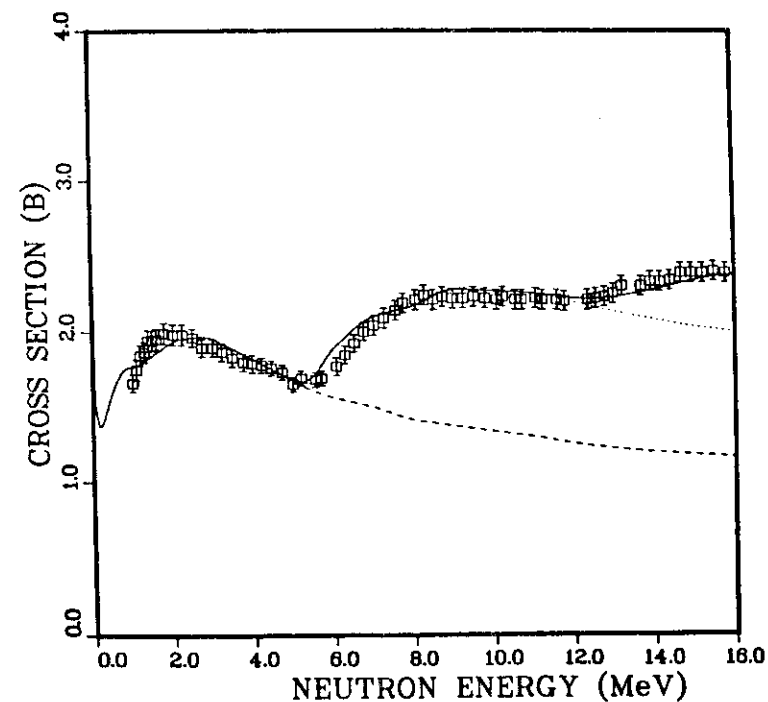


Fig. 6. Calculated $n + ^{239}\text{Pu}$ total fission cross sections (solid curve) compared with the data of Karl et al.²⁹ The dashed and dotted curves indicate the calculated behavior of the second-chance fission and the second- and third-chance fission sum.

40